

An excess of mid-IR luminous galaxies in Abell 1689?*

D. Fadda¹, D. Elbaz¹, P.-A. Duc^{2,3}, H. Flores¹, A. Franceschini⁴, C.J. Cesarsky⁵, and A.F.M. Moorwood⁵

¹ CEA Saclay – Service d’Astrophysique, Orme des Merisiers, 91191 Gif-sur-Yvette Cédex, France

² CNRS URA 2052 and CEA Saclay – Service d’Astrophysique, Orme des Merisiers, 91191 Gif-sur-Yvette Cédex, France

³ University of Cambridge, Institute of Astronomy, Madingley Road, Cambridge, CB3 0HA, UK

⁴ Dipartimento di Astronomia, Università di Padova, Vicolo dell’Osservatorio, 5, 35122 Padova, Italy

⁵ European Southern Observatory, Karl-Schwarzschild-Strasse 2, 85748 Garching bei München, Germany

Received 29 February 2000 / Accepted 20 July 2000

Abstract. We present the results of infrared observations of Abell 1689, an exceptionally rich cluster of galaxies at intermediate redshift ($z \simeq 0.181$). It was observed with ISOCAM, at $6.7 \mu\text{m}$ and $15 \mu\text{m}$, and ISOPHOT at $200 \mu\text{m}$ from the *Infrared Space Observatory* (ISO). The cluster galaxies detected above a sensitivity limit of 0.15 mJy in the $6.7 \mu\text{m}$ band, whose emission is mostly dominated by their stellar component, show optical colors similar to the overall cluster population and are gathered in the center of the cluster, following the distribution of the cluster early-types. In the $15 \mu\text{m}$ band, above a sensitivity limit of 0.3 mJy , the galaxies spectroscopically confirmed to be cluster members are blue outliers of the cluster color-magnitude relation and become brighter going from the center to the outer parts of the cluster.

We compare the $6.7 \mu\text{m}$ and $15 \mu\text{m}$ fluxes and the cumulative distributions of the B-[6.75] and B-[15] colors of the A1689 galaxies, above our 90% completeness limits of 0.2 and 0.4 mJy for $6.7 \mu\text{m}$ and $15 \mu\text{m}$ respectively, to the galaxies of two nearby clusters, Virgo and Coma, and to the field galaxies at the same redshift of the cluster. Although the B-[6.7] color distributions of the three clusters are compatible, we find a systematic excess of B-[15] color distribution for the galaxies located in Abell 1689 with respect to Coma or Virgo galaxies. This result proves the existence of a mid-infrared equivalent of the Butcher-Oemler effect measured in the optical. The comparison of $15 \mu\text{m}$ flux and B-[15] color distributions of A1689 and field galaxies does not show strong differences between the population of starburst galaxies in the cluster and in the field.

Key words: galaxies: clusters: individual: A 1689 – galaxies: evolution – cosmology: observations – infrared: galaxies

Send offprint requests to: D. Fadda (dfadda@cea.fr)

* Based on observations with ISO, an ESA project with instruments funded by ESA Member States (especially the PI countries: France, Germany, the Netherlands and the United Kingdom) with the participation of ISAS and NASA

1. Introduction

The first evidence for an increase of the star formation activity in galaxies within high redshift clusters with respect to nearby clusters was the discovery of an increasing fraction of blue galaxies with cluster redshift (Butcher & Oemler 1978, 1984). This effect was later confirmed by other photometric studies (e.g. Couch & Newell 1984, Rakos & Schombert 1995, Lubin 1996, Margoniner & de Carvalho 2000) and searches for spectroscopic signatures of the star formation activity (Couch & Sharples 1987, Dressler et al. 1985, Dressler & Gunn 1992).

All these studies are limited to optical data and thus they have no access to the global star formation activity. Only infrared or radio data (see e.g. Smail et al. 1999) can in fact reveal the part of star formation activity hidden by dust. But up to now, the Butcher-Oemler effect has never been studied in the mid-infrared. The high sensitivity and resolution of ISOCAM (Cesarsky et al. 1996a) on board of the ISO satellite (Kessler et al. 1996) has allowed the MIR observation of galaxies in distant clusters for the first time. The analysis of these new data will shed new light on this issue and constrain the model predictions.

The usual scenario to explain the Butcher-Oemler effect invokes the interaction of infalling galaxies with the dense cluster environment. However, the specific role of the environment on the activity of these galaxies has been subject to debate since it could either enhance star formation or, on the contrary, quench it. Indeed, star formation could be triggered by galaxy-galaxy interaction (e.g. Lavery & Henry 1986), galaxy harassment (Moore et al. 1996) or interaction with the intra-cluster medium (ICM, see Gunn & Gott 1972; Gavazzi & Jaffe 1987), but it could also be quenched by ram pressure or tidal stripping (e.g. Ghigna et al. 1998, Ramirez & de Souza 1998, Fujita & Nagashima 1999).

Comparing a large sample of galaxies in medium-redshifts clusters to field galaxies, Balogh et al. (1998) found that galaxies with similar bulge-to-total luminosity ratio show stronger $[OII]\lambda 3727$ equivalent widths, hence higher star formation rates, in the field than in clusters. They conclude that the dense environment of cluster galaxies quenches their star formation activity, independently on the morphological type of the galax-

ies. Abraham et al. (1996) reached the same conclusion in the study of a large strip of sky centered on the rich cluster Abell 2390 ($z = 0.23$).

Dressler et al. (1999) observed another sample of ten distant rich galaxy clusters. Using HST images to deduce the galaxy morphologies, they definitively proved that cluster galaxies have reduced star formation with respect to field galaxies with the same morphological types.

Galaxies with no strong dust extinction show a correlation of their MIR flux densities with UV (Boselli et al. 1997) or $H\alpha$ (Roussel et al. 2000). However, the strongest starbursts known do not present such correlation because they are heavily extinguished (Rigopoulou et al. 1999) and they emit most of their light in the infrared (Sanders & Mirabel 1996). Poggianti & Wu (2000) have shown that almost 50% of very luminous IR galaxies present spectra with both strong $H\delta$ in absorption and relative modest [OII] emission. These galaxies, thought to be dusty starburst, are detected also in distant clusters (Poggianti et al. 1999) and are expected to be easily detectable by ISOCAM in the clusters as well as in the case of deep fields (see Flores et al. 1999).

To explore the role of the cluster environment in galaxy evolution we have therefore performed a survey of clusters from the nearby universe to $z \sim 1$ (Fadda & Elbaz 1998). In this paper, we present the results of our MIR and FIR observations of Abell 1689, an exceptionally rich cluster of galaxies at $z=0.181$ (Struble & Rood 1987), with respectively ISOCAM and ISOPHOT (Lemke et al. 1996) on-board ISO.

Although the evolution of the fraction of blue galaxies at low redshifts ($0.1 < z < 0.2$) is not yet well established (see Butcher & Oemler 1984, Rakos & Schombert 1995 and Margoniner & de Carvalho 2000), A1689 shows a clear Butcher-Oemler effect since its fraction of blue galaxies is about three times higher than in nearby clusters (Butcher & Oemler 1984). This value, which has been questioned by the study of Gudehus & Hegyi (1991), has been recently confirmed by Margoniner & de Carvalho (2000).

We compare in the present paper the star formation activity, based on MIR fluxes, of the Abell 1689 galaxies with that in the nearby rich clusters Coma and Virgo.

After the presentation of the MIR observations and data reduction, we describe the IR properties of the A1689 galaxies through their radial and color distribution, we compare their MIR luminosity functions with those of the Coma and Virgo clusters and of field galaxies. In a companion paper (Duc et al. 2000), we will present the optical follow-up observations and an analysis of the spectral properties, morphology and star formation of the galaxies detected. Throughout all the paper, we assume $q_0 = 0.5$ and $H_0 = 75 \text{ km s}^{-1} \text{ Mpc}^{-1}$.

2. Observations and data reduction

2.1. Observations

Abell 1689 has been observed with ISO as part of a program of observations of distant galaxy clusters (DEEPZCLS, P.I.: A. Franceschini). The observations were performed in the two

Table 1. ISOCAM Observations of A1689 presented in the paper. Asterisks mark observations executed during the performance verification phase. We report the area observed, the number of raster pointings or frames (N_f), the number of readouts per pointing (N_r) or ramps in the case of C200, the integration time, the pixel field of view and the observation number in the ISO archive.

Filter	Field	N_f	N_r	T_{int}	PFoV	Obs. Nr.
CAM-LW3*	6'x6'	9	419	5s	6''	06600703
CAM-LW3*	6'x6'	9	308	10s	6''	06600602
CAM-LW2*	6'x6'	9	292	10s	6''	07000407
CAM-LW3	5'x5'	16	462	10s	6''	25402507
CAM-LW2	5'x5'	16	462	10s	6''	25402507
PHT-C200	9'x12'	6	16	32s	90''	40100233

MIR bands LW2 and LW3 which cover the spectral regions 5.0–8.3 μm and 11.6–18.0 μm , respectively and are centered at 6.75 μm and 15 μm . Additionally, the cluster was observed in the broad FIR band C200 which covers the spectral region 187–217 μm and is centered at 200 μm . Table 1 summarizes the main features of these observations.

The field has been covered with subsequent pointings of the ISO camera (raster). For each pointing, ~ 25 readouts were performed since the detector needs a time to stabilize which depends on the mean flux and on the flux of the source. Since Abell 1689 is near to the ecliptic plane ($\lambda = 197.00$, $\beta = 5.78$) where the zodiacal light is intense, the mean flux is high and the signal always reaches stabilization (Coulais & Abergel 1999).

Some observations of A1689 were performed during the performance verification phase of the ISO mission in order to determine the best combination of parameters to observe faint sources with ISOCAM. We have used only three of these observations, because the quality of the other is very poor.

The total time spent for each pixel of the final image, which takes into account all the rasters coadded, is about 25 minutes for the LW2 filter, 30 minutes for the LW3 filter and 77 seconds for the C200 filter.

2.2. Data reduction

The data reduction can be summarized in the following steps:

- dark subtraction, using the time-dependent dark correction in the CIA¹ package (Biviano et al., 1999);
- deglitching of short glitches due to low energy cosmic rays, using the Multi-resolution Median Transform technique (Starck et al., 1999);
- removal of long glitch tails due to high energy cosmic rays, mainly using the PRETI algorithm (Starck et al., 1999);
- flat fielding and baseline subtraction to remove the long term transients in pixel signals, using the PRETI algorithm;

¹ CIA is a joint development by the ESA Astrophysics Division and the ISOCAM Consortium. The ISOCAM Consortium is led by the ISOCAM PI, C. Cesarsky, Direction des Sciences de la Matière, C.E.A., France.

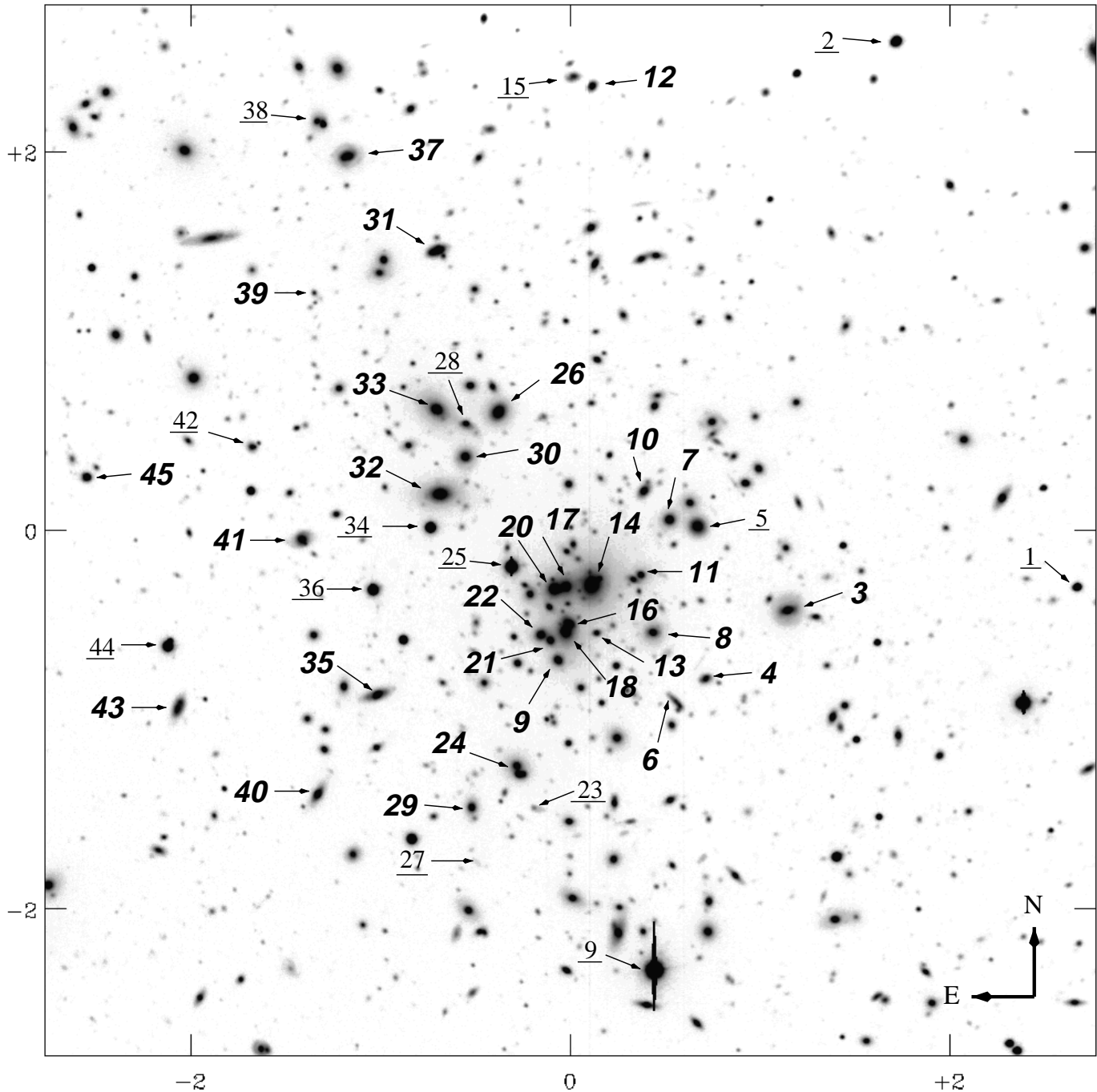


Fig. 1. Finding chart of the sources detected by ISOCAM. The image was taken at the NTT in the R band (see Duc et al. 2000). Galaxies identified by their numbers are listed in Table 2. Bold slanted numbers indicate confirmed cluster members. Units for the axes are arcminutes.

(e) coaddition of mosaic images, taking into account the camera distortion (Aussel et al. 1999), to obtain a final image with a pixel size of 2 arcsec.

Some further improvements, described below, have been added to this process in order to best exploit this data set.

We have not considered some noisy data: we have masked the border pixels which are badly illuminated and we have not taken into account the first readouts when the signal is not yet stabilized. Indeed, as an observation begins, the flux on the de-

tektor changes rapidly and exhibits a transient behavior with an artifact which can mimic a source, hence we mask the first readouts for each pixel (see Fig. 4).

After a deep negative tail which follows the impact of an energetic cosmic ray (see Starck et al., 1999), the detectors sometimes produce a bump resembling a source. While it is easy for PRETI to remove the negative oscillations, the first positive bump of the signal often has the same temporal size as a typical source (see Fig. 5). Thus, when PRETI decomposes the signal in

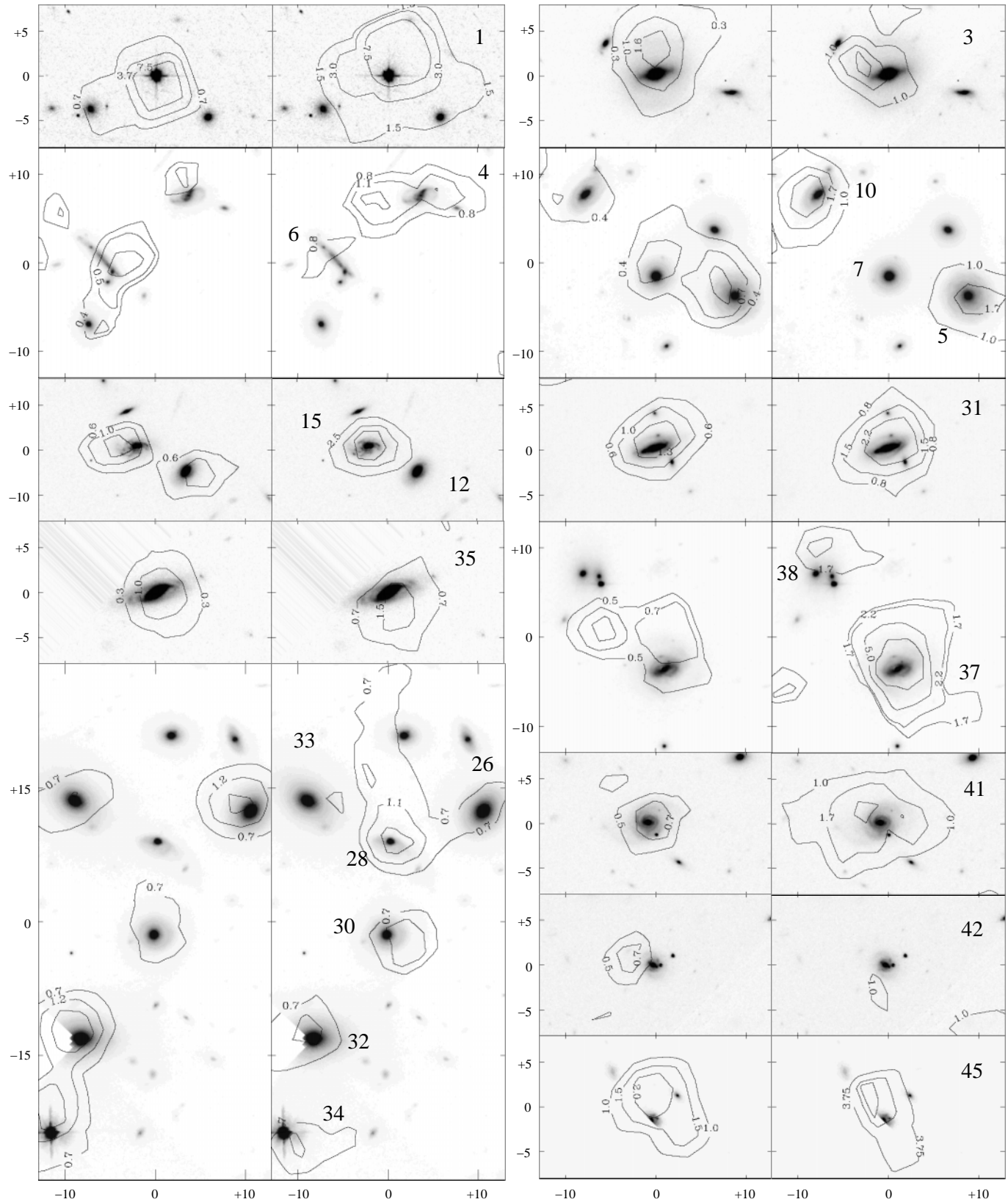


Fig. 2. Galaxies detected with the LW2 and LW3 filters out of the cluster center on HST images. For each galaxy, LW2 and LW3 contours are on the left and on the right, respectively. Contour levels are expressed in $\mu\text{Jy arcsec}^{-2}$, while axes units are in arcseconds. Numbers refer to Table 2.

Table 2. List of sources

Id. Nr. (1)	Optical counterpart		B (4)	R (5)	z (6)	Mem- ber- ship (7)	LW2		SNR (10)	p (11)	LW3		SNR (14)	p (15)	
	RA (2000) (2)	DEC (2000) (3)					offset (arcsec) (8)	flux (μ Jy) (9)			offset (arcsec) (12)	flux (μ Jy) (13)			
1	13:11:19.18	-1:20:31.6	18.8	18.0	2.584	B	+0.0	-0.4	870 \pm 120	16	<.001	-1.1 + 2.1	2600 \pm 360	16	<.001
2	13:11:22.82	-1:17:37.8	18.2	15.8	0	S	+2.4	-1.2	1300 \pm 140	20	<.001		< 770		
3	13:11:25.31	-1:20:37.7	19.8	17.4	0.192	M	-0.3	+2.6	313 \pm 70	8	0.001	+3.0 + 1.7	450 \pm 180	5	0.001
4	13:11:27.07	-1:20:59.0	20.8	19.1	0.215	M	+0.6	+1.3	< 120	2	0.003	+1.3 - 1.1	320 \pm 230	4	<.001
5	13:11:27.19	-1:20:10.6	19.4	17.6	0.086	F	+1.6	+1.6	190 \pm 70	7	0.001	-2.0 - 1.1	440 \pm 180	5	<.001
6	13:11:27.69	-1:21:06.7	20.6	19.1	0.216	M	-3.3	-1.3	190 \pm 70	5	0.001	+1.4 - 1.0	< 280	2	0.004
7	13:11:27.78	-1:20:08.4	20.3	17.8	0.19 ^{ph}	M	-0.8	+2.4	190 \pm 70	6	0.001		< 280		
8	13:11:28.16	-1:20:44.1	20.3	18.0	0.171	M	+2.2	-1.5	260 \pm 70	7	0.003		< 280		
9	13:11:28.24	-1:22:31.1	14.6	<14	0	S	+0.9	+0.5	1770 \pm 180	48	<.001		< 360		
10	13:11:28.30	-1:19:59.0	20.3	18.3	0.178	M	+1.0	-1.0	200 \pm 70	6	<.001	+0.8 - 0.9	600 \pm 190	7	<.001
11	13:11:28.40	-1:20:25.7	21.1	18.5	0.20 ^{ph}	M	+0.5	-0.3	200 \pm 70	6	<.001		< 280		
12	13:11:29.27	-1:17:50.5	20.3	18.8	0.173	M	-1.4	+0.4	190 \pm 70	3	<.001		< 360		
13	13:11:29.38	-1:20:43.9	21.0	18.6	0.18 ^{ph}	M	*		130 \pm 70	4	*		< 280		
14	13:11:29.44	-1:20:28.5	18.4	16.0	0.184	M	*		490 \pm 90	17	*	-2.9 + 2.1	460 \pm 180	5	<.001
15	13:11:29.67	-1:17:47.6	21.0	19.0	0.397	B	+2.1	+0.4	190 \pm 70	3	<.001	-0.2 + 0.5	900 \pm 170	6	<.001
16	13:11:29.94	-1:20:40.8	19.8	18.1	0.200	M	*		300 \pm 70	9	*		< 280		
17	13:11:29.99	-1:20:29.2	20.4	17.8	0.19 ^{ph}	M	*		300 \pm 70	9	*	-0.2 - 2.4	430 \pm 190	5	0.001
18	13:11:30.01	-1:20:43.4	18.9	17.3	0.204	M	*		230 \pm 70	7	*		< 280		
19	13:11:30.17	-1:20:52.3	20.4	17.7	0.19 ^{ph}	M	*		170 \pm 70	5	*		< 280		
20	13:11:30.22	-1:20:29.8	19.5	17.2	0.174	M	*		400 \pm 80	13	*		< 280		
21	13:11:30.34	-1:20:46.0	20.9	18.2	0.19 ^{ph}	M	*		220 \pm 70	6	*	-1.5 - 1.5	330 \pm 230	4	0.002
22	13:11:30.53	-1:20:44.3	20.4	17.9	0.192	M	*		100 \pm 60	4	*		< 280		
23	13:11:30.69	-1:21:39.3	21.9	20.6	0.692	B			< 100			+3.2 + 0.3	340 \pm 220	4	0.020
24	13:11:31.08	-1:21:25.8	20.9	18.3	0.197	M	-1.9	+0.9	200 \pm 70	6	0.001		< 280		
25	13:11:31.13	-1:20:22.6	15.9	15.3	0	S	+0.9	+1.5	290 \pm 70	9	<.001		< 280		
26	13:11:31.36	-1:19:33.5	19.5	17.0	0.188	M	+0.4	+0.4	330 \pm 70	11	<.001	-0.6 + 0.6	< 280	3	<.001
27	13:11:31.99	-1:21:55.9	-	21.6	0.87 ^{ph}	B			< 110			-0.6 - 0.8	820 \pm 170	8	0.005
28	13:11:32.04	-1:19:37.3	20.2	18.7	0.15 ^{ph}	M?			< 90			-0.5 + 0.4	400 \pm 200	5	0.001
29	13:11:32.05	-1:21:38.8	20.6	18.3	0.177	M	+2.1	+0.6	100 \pm 60	3	<.001		< 280		
30	13:11:32.07	-1:19:47.6	20.4	17.7	0.180	M	+0.0	+2.1	210 \pm 70	7	<.001	-3.4 - 1.2	< 280	3	0.001
31	13:11:32.60	-1:18:42.2	19.4	17.6	0.176	M	+0.0	+1.0	110 \pm 60	3	<.001	+0.4 + 0.7	600 \pm 190	6	<.001
32	13:11:32.61	-1:19:59.3	19.1	16.6	0.202	M	+1.0	+0.8	350 \pm 70	13	<.001	+0.2 + 1.8	< 280	3	<.001
33	13:11:32.66	-1:19:32.5	19.5	16.8	0.201	M	+0.2	-0.3	230 \pm 70	7	<.001		< 280		
34	13:11:32.83	-1:20:09.8	17.2	16.0	0	S	-0.4	+2.1	320 \pm 70	15	<.001	-1.7 - 1.1	< 280	2	
35	13:11:34.02	-1:21:02.6	19.7	17.9	0.181	M	-1.5	-0.4	210 \pm 70	6	0.001	-0.9 - 0.3	< 400	3	0.001
36	13:11:34.06	-1:20:29.3	17.3	15.9	0	S	-0.9	+1.0	240 \pm 70	8	<.001		< 280		
37	13:11:34.47	-1:18:11.8	19.7	17.7	0.199	M	-2.3	+2.6	220 \pm 70	4	0.002	-1.0 + 0.8	1970 \pm 300	16	<.001
38	13:11:35.09	-1:18:00.4	22.5:	19.1	-	?			< 170			-0.9 + 2.9	680 \pm 190	5	0.006
39	13:11:35.20	-1:18:55.1	22.6	20.4	0.19 ^{ph}	M			< 130			-1.2 - 0.7	370 \pm 210	4	0.012
40	13:11:35.30	-1:21:33.8	20.4	17.9	0.187	M	+0.6	+4.7	150 \pm 70	4	0.003		< 280		
41	13:11:35.55	-1:20:13.0	19.9	18.3	0.200	M	-1.2	+1.1	190 \pm 70	5	<.001	-0.2 + 1.0	790 \pm 170	8	<.001
42	13:11:36.55	-1:19:43.4	21.1	19.3	0.13 ^{ph}	F?	+3.2	+0.5	110 \pm 60	3	0.004	+1.1 - 2.7	< 280	3	0.009
43	13:11:38.21	-1:21:05.7	20.2	18.2	0.196	M	-4.9	+1.9	160 \pm 70	4	0.008		< 280		
44	13:11:38.40	-1:20:46.2	17.3	15.7	0	S	-2.0	+0.5	450 \pm 80	11	<.001		< 320		
45	13:11:40.07	-1:19:52.3	19.9	18.7	0.188	M	+0.1	+2.6	490 \pm 90	10	0.002	+1.4 + 2.1	1230 \pm 220	7	0.001

Comments: For each detection we list: the identification number (Column 1), the coordinates of the optical counterpart (Columns 2 and 3), the B and R magnitudes (Columns 4 and 5), the redshift (Column 6) and the membership (Column 7: M = member, F = foreground, B = background, S = star). The B filter corresponds to the B_b filter of the EMMI camera on the ESO-NTT telescope. For the two ISOCAM filters we report the offset (Columns 8 and 12) from the optical counterpart, the flux with the error (or the 3σ upper limit, Columns 9 and 13), the signal to noise ratio (Columns 10 and 14) and the probability of spurious identification, p (Columns 11 and 15). Asterisks in Column 11 mark LW2 sources in the central concentration which have been deconvolved. While the SNR is computed on the image, the flux error is dominated by the uncertainty in the correction factor computed through simulations (see Fig. 8 and the text). All the redshifts are from Duc et al. (2000), except for #1, which is a QSO, from Hewett et al. (1995), #29, from Teague et al. (1990) and photometric redshifts (marked with a *ph*) from Dye et al. (2000).

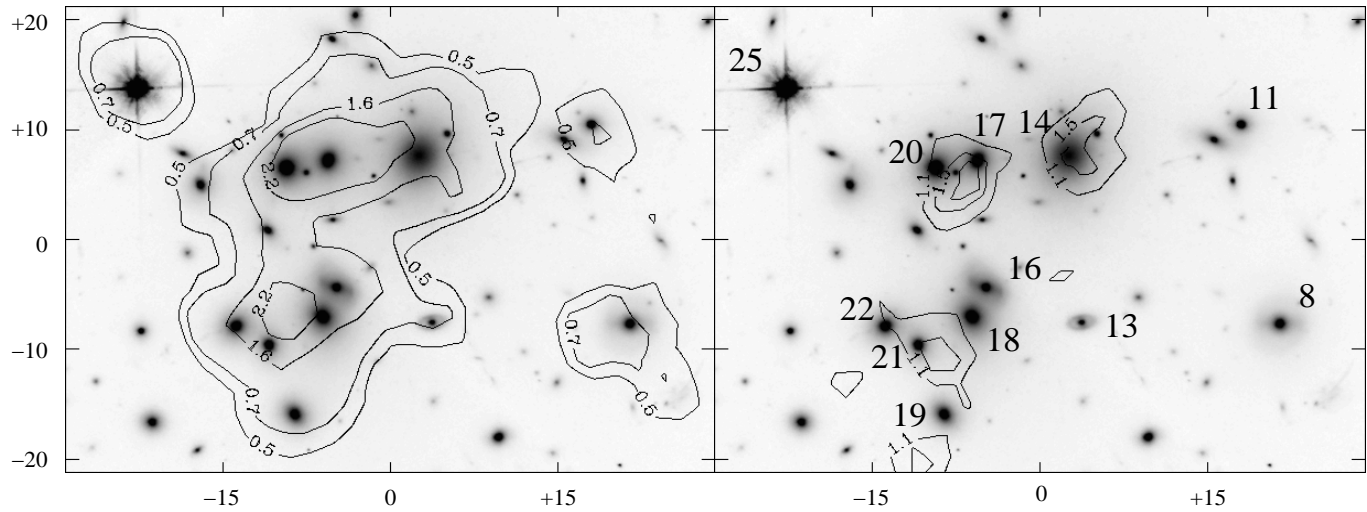


Fig. 3. HST image of the central crowded area of A1689 superposed with LW2 (left) and LW3 (right) contours. Contour levels are expressed in $\mu\text{Jy arcsec}^{-2}$ and axes units in arcseconds. Galaxies identified by their numbers are listed in Table 2.

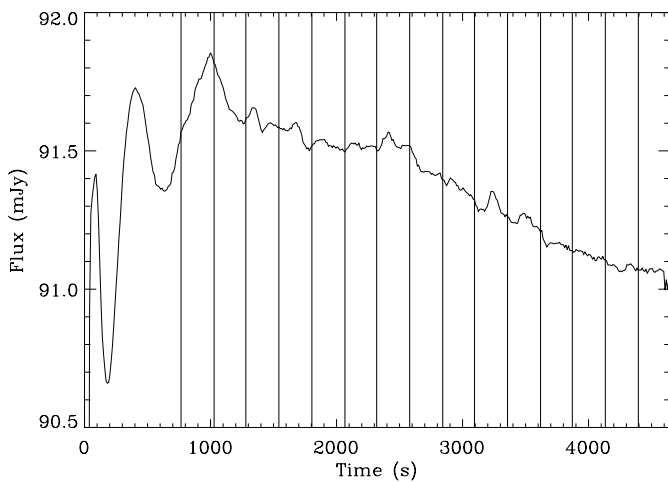


Fig. 4. The initial transient in the case of an LW3 observation of the cluster as seen in the median behavior of all the camera pixels. Vertical lines indicate the moment when the camera changes its pointing during the raster. After an initial increase in the flux there are some oscillations. The first 70 readouts (almost 800 seconds) are the so called stabilization time which is rejected in the analysis. In this case, we reject other two pointings because of a further bump in the signal. Then, the drift in the signal is easily corrected by the PRETI software.

components of different temporal scales, it classifies this bump as a source introducing false detections. Unfortunately, due to the large variety of cases and the presence of several glitches at the same time, it is very difficult to correct the signal by modeling these type of glitches. Therefore, we have decided to subtract from the signal each positive component of the PRETI analyses which comes exactly after the negative tail of a glitch.

Transient effects appear during and after observing a source because of the inertia of the detector. The initial transient depends on the mean flux and on the flux of the source and can affect the flux measured. In our case the mean flux is high because we are observing an object near the ecliptic plan where

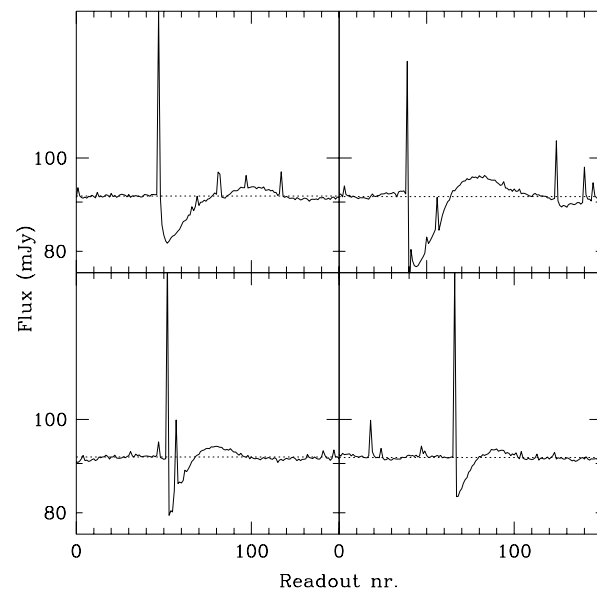


Fig. 5. Four examples of oscillations in the signal after an impact of an energetic cosmic ray on the camera. After the glitch and its negative tail the signal returns to the median value (dashed line) passing through a positive bump that can be interpreted as a source.

the zodiacal light is intense and the signal reaches stabilization after few readouts (Coulais & Abergel 1999). Therefore, we do not correct for this effect. Tails, which appear after the detection of bright sources, can generate artificial sources (ghosts) in the final image. Since transient correction techniques (Coulais & Abergel 1999) are not yet well suited to correct this effect in the case of bright point sources, we simply removed these tails from the signal.

Astrometry corrections must be made before coadding several independent observations. Since the error in the angular position of the camera is negligible, the astrometry correction reduces to an offset. To estimate the offsets we compare the

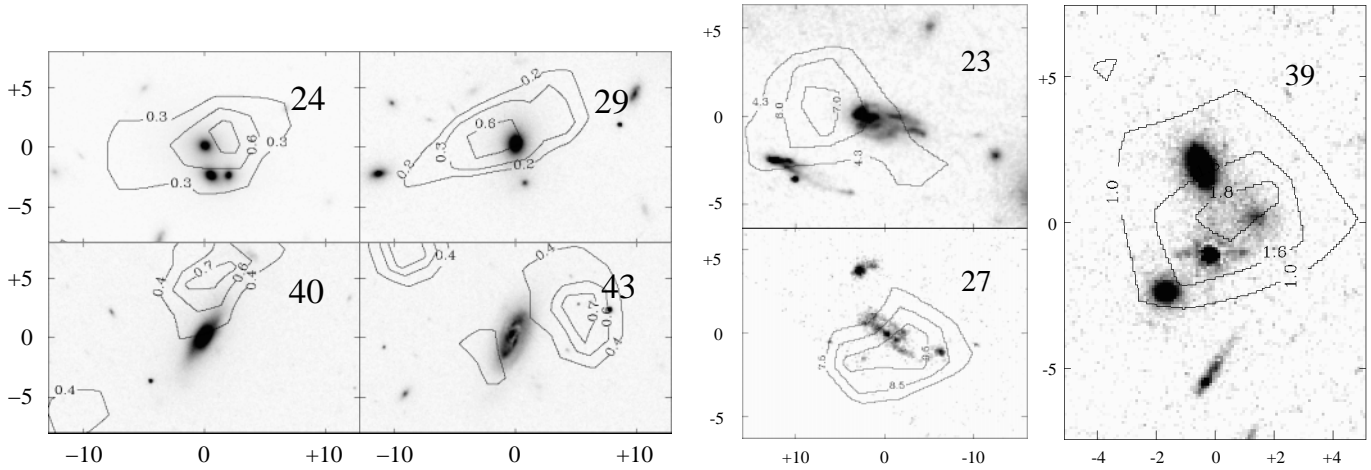


Fig. 6. HST images of galaxies detected only with the LW2 (left) or the LW3 (right) filter. Contour levels are expressed in $\mu\text{Jy arcsec}^{-2}$, while axes units are in arcseconds. Numbers refer to Table 2. Detections of #40 and #43 present large offsets because they are at the border of the field where redundancy is lower and distortion effects become important. The optical counterparts of #23 and #27, high redshift objects detected in the LW3 band, have distorted morphologies.

Table 3. Statistics of ISO detections.

Filter	N_{src}	N_z	$N_{members}$	N_{bkg}	N_{stars}
LW2	30 (39)	30 (39)	20(29)	4	6
LW3	18	17	12	5	0
LW2&LW3	12 (20)	12 (20)	9(14)	3(6)	(1)

Comments: LW2 sources have been detected at the 3σ level, LW3 sources at the 4σ level. In the LW2 line, the numbers in parentheses include the LW2 sources in the central region, which have been deblended. In the LW2&LW3 line, the numbers in parentheses include also counterparts of LW2 or LW3 sources which have been detected at a lower σ level than the previous ones.

ISO images with an optical image and we evaluate the coordinate shifts of bright optical sources which are detected in the field. Offset corrections are 2 arcsecs on average.

3. Data analysis

3.1. Source detection and optical counterparts

We extract sources from the final image using the corresponding rms map computed by PRETI (Starck et al., 1999) which takes into account the history of the signal for each pixel. The use of the rms map in this step is very important, because the sensitivity changes from point to point due to the variable number of camera pointings and of the number of the readouts which have been masked to remove glitches.

To extract sources we consider the signal-to-noise ratio (SNR) map computed using the ratio of the image and corresponding rms map and we consider all the peaks greater than 3. We retain these sources if the SNR computed for a region of 8 arcsec radius is still greater than 3 for the LW2 sources. For LW3 we choose a more conservative level ($\text{SNR} > 4$) due to the higher frequency of glitches.

After astrometry corrections, the error in global astrometry is remarkably small: less than or equal to 2 arcsec. This allows us to identify ISO sources with corresponding optical sources with a high confidence level (see Figs. 2, 3, 6). To find optical counterparts we have used a large field R-band image obtained with the NTT at La Silla and images from the HST archive. For most of the galaxies detected we have also obtained spectra with EMMI on the NTT (Duc et al., 2000). Optical counterparts are assigned with the method described by Downes et al. (1986). For each source, we consider candidates in the R-band image within a radius which depends on the resolution of the observation (e.g. 6 arcseconds in the case of our LW3 image). Taking into account the fact that bright optical sources are more easily detected than faint ones, the method assigns to each candidate the probability of spurious identification. This method works well with point sources as in our case.

For each detection, we report in Table 2 the position of the optical counterpart, its B and R magnitudes, the spectroscopic or photometric redshift, the membership, the offsets from the optical counterpart, the flux, the signal-to-noise ratio, and the probability of spurious association with the optical source. If one source is only detected in the LW2 (with $\text{SNR} > 3$) or in the LW3 (with $\text{SNR} > 4$) filter we report the detection at lower SNR level in the other band too. In case of no detection we report an upper limit (see below).

In the center of the LW2 image (see Fig. 3), several sources are blended into one extended source. To estimate the flux of the individual galaxies, we have assumed that the brightest optical galaxies emit in the LW2 band. Then we have fitted ISOCAM point spread functions at the positions of these sources by choosing the fluxes which minimize the residual flux. LW2 fluxes obtained in such a way are reported in Table 2.

Table 3 summarizes the statistics of ISOCAM detections. We report, for each band, the number of detections with optical counterparts, the number of sources with known redshift, the

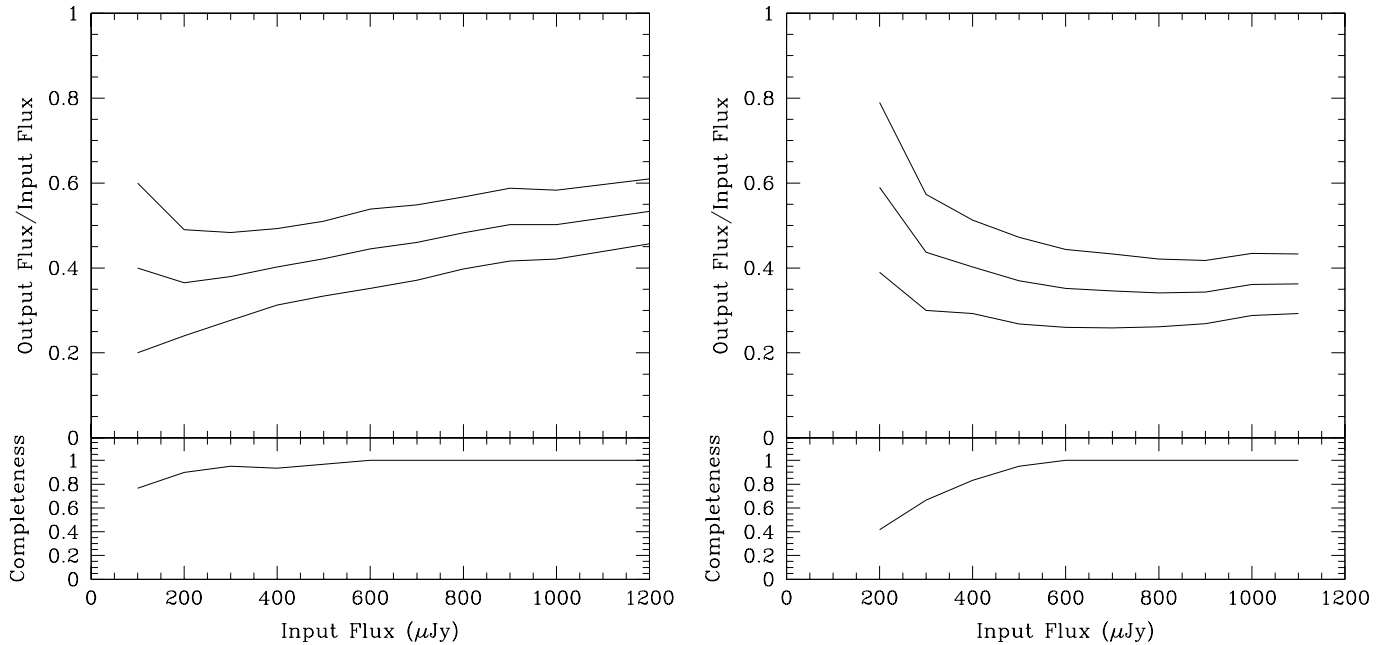


Fig. 7. Photometry and completeness results for LW2 (right) and LW3 (left) fluxes obtained through simulations. Top: the ratio between measured and input flux as a function of input flux with 1σ error bands. Bottom: percentage of detected sources in simulations as a function of the input flux of the sources (at 3σ level for LW2 and 4σ level for LW3).

spectroscopically confirmed number of cluster members and background galaxies and the number of stars detected.

A large number of detected galaxies are cluster members (88% of LW2 sources and 66% of LW3 sources), in contrast to that found by Altieri et al. (1999) who found mainly lensed background galaxies for the core of A2390. The reason for this discrepancy is probably that deep images were obtained by Altieri et al. for the very central part of A2390, while the majority of the MIR cluster galaxies, harboring dust obscured star formation, lie in the outskirts (see our results below).

3.2. Photometry and completeness

Once the source positions are obtained, we performed aperture photometry on the coadded image within a circle of radius 8 arcsec. The fluxes obtained take into account only part of the PSF, because the wings of the PSF are confused in the noise. This effect depends on the source flux and the wavelength. We have corrected the measured fluxes through simulations.

Simulations are made by introducing artificial sources in a zone which is observed at least 25 minutes in the case of LW2 observations and 30 minutes for the LW3 observations. This region covers most of the sources detected, except for few external high flux sources. Choosing the positions we avoid regions with $\text{SNR} > 2$. We actually add these sources to the original data cube by taking into account all the effects which enter in the real signal (dark current, flat-field, transients, point spread functions and camera distortions). We must use real data because a complete model of noise including cosmic ray effects does not exist. Then we analyze this new cube exactly in the same manner as the real data and we measure fluxes for sources

which are detected. In this way we are able to produce a curve (see Fig. 7) which is used to correct measured fluxes and assign an error or evaluate an upper limit. The uncertainty of this correction dominates the error in the flux evaluation on the image. In Table 2 we report this error, while the SNR is computed on the image. Therefore, also detections with high SNR can have big photometric errors, especially in the case of low fluxes.

These simulations also allowed us to estimate the sensitivity limit and the completeness for the two filters. In the LW2 band, it is possible to detect sources to a sensitivity limit of 0.15 mJy while the 100% completeness level is reached at 0.4 mJy. The LW3 image, which is noisier than the LW2 image due to higher zodiacal light contribution, has a sensitivity limit of 0.3 mJy and is 100% complete above 0.6 mJy.

4. Results

The ISOCAM filters, LW2 and LW3, were designed to sample two dominant components of the rest-frame MIR emission: broad bands whose carriers are aromatic carbon compounds (hereafter called aromatic features) and a continuum radiated by hot ($\sim 100\text{ K}$) small dust grains stochastically heated (Cesarsky et al. 1996a). Template spectral emission distributions (SED) observed by the ISOCAM CVF for different types of galaxies are shown in Fig. 8. The spectral ranges of the SEDs observed by the LW2 and LW3 filters are shown by bold lines. The evolved stellar population dominates the emission of a typical elliptical galaxy which does not exhibit MIR features. Late-type galaxies show the aromatic features and the dust continuum whose relative contribution increases with star formation activity. At the redshift of A1689, the LW2 filter can cover the tail

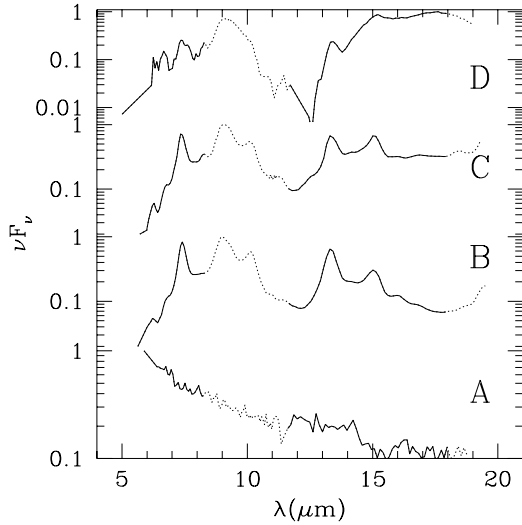


Fig. 8. MIR SEDs of: A) the elliptical galaxy NGC 1399 (Madden et al., 1999), B) the galactic photodissociation region NGC 7023 (Cesarsky et al., 1996b), C) the starburst M 82 (Tran, 1998) and D) the ULIRG Arp 220 (Charmandaris et al., 1999) placed at the redshift of A1689 ($z = 0.181$). νF_ν is in arbitrary units. Bold lines correspond to the spectral ranges seen by the two ISOCAM filters LW2 (on the left) and LW3 (on the right).

of stellar emission and the $6.7 \mu\text{m}$ aromatic feature. The LW3 band covers the $11.3 \mu\text{m}$ and $12.6 \mu\text{m}$ aromatic features and the hot dust continuum, which can dominate in galaxies with a high star formation rate.

4.1. Radial distribution

A rich, relaxed and unperturbed cluster has a radially decreasing density profile of galaxies. The distribution of galaxies with peculiar properties can exhibit a spatial segregation, e.g. morphological (e.g. Dressler 1980) or a luminosity segregation (e.g. Biviano et al. 1992). In particular, starburst galaxies tend to be more frequent in the outskirts of clusters as well as the blue galaxies which are responsible for the Butcher-Oemler effect (Butcher & Oemler 1984, Abraham et al. 1996, Rakos et al. 1997, Ellingson et al. 1999). At the same time, emission line galaxies and blue galaxies have higher velocity dispersions and steeper velocity dispersion profiles than quiescent and red galaxies, respectively (Biviano et al. 1997, Carlberg et al. 1997), suggesting that star-forming galaxies are falling into the cluster, maybe for the first time.

For this reason we explored the relationship between the fluxes of ISOCAM galaxies in the two bands and their distance from the cluster center within the radius of ~ 0.5 Mpc, which roughly corresponds to 2 core radii. Fig. 9 reports, for the cluster members detected in the two bands, fluxes and colors as a function of the radius and the spatial distributions of the detections. Median values and 1σ error bands have been computed for fluxes and colors divided in three bins. Dispersions have been computed using the bootstrap technique and taking into account also upper limits in the case of color diagrams. The figure shows

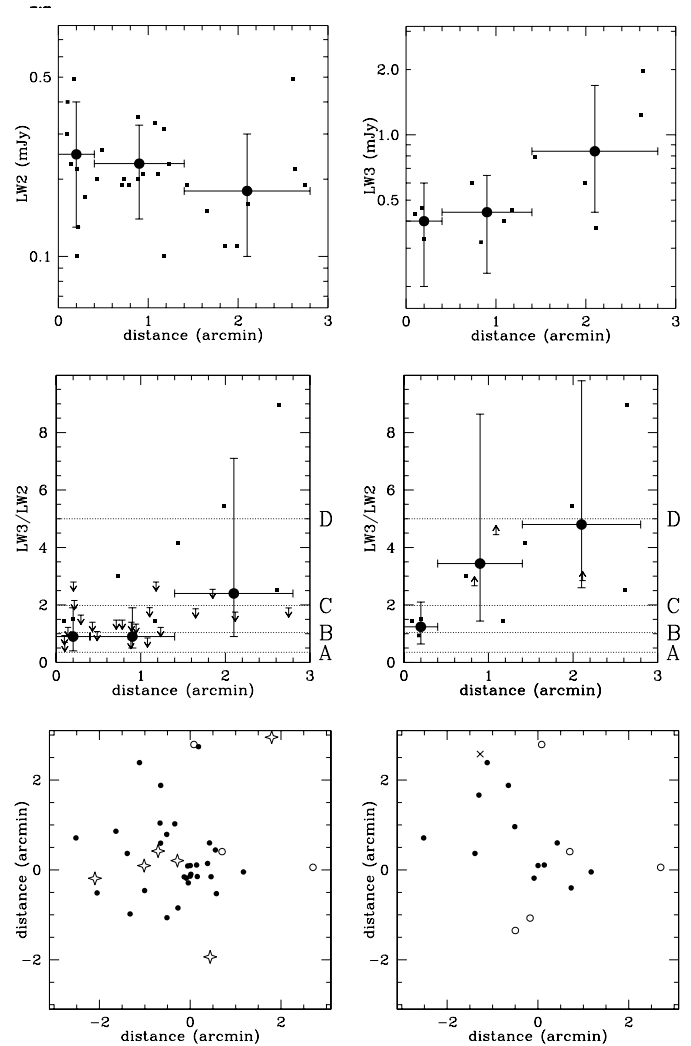


Fig. 9. On the top: fluxes of confirmed member galaxies detected with the two filters as a function of distance to the cluster center. On the center: LW3/LW2 color versus the distance to the cluster center for LW2 (left) and LW3 (right) detections including upper limits. Fluxes and colors are binned in three bins and bootstrap technique has been used to evaluate 1σ error-bands. Points mark fluxes or LW3/LW2 ratios for individual galaxies. Colors of template galaxies in Fig. 8 are reported for reference (LW3/LW2 = 0.4, 1.0, 2.0 and 5 for A, B, C and D template, respectively). On the bottom: the spatial distribution of LW2 (left) and LW3 (right) detections. Confirmed cluster members are filled circles, background galaxies are empty circles, starlike symbols are stars and finally crosses are galaxies with unknown redshift.

that the majority of bright LW2 sources are concentrated in the central region: 75% of the sources within 1.3 arcminutes are brighter than 0.2 mJy, while 70% of the sources in the external region are fainter than 0.2 mJy. If we take into account that the sensitivity of the observations decreases far from the cluster center, the real effect is even stronger than our measurements indicate. We can understand this fact because LW2 detections correspond to the brightest optical galaxies, since LW2 emission is dominated by stellar emission, and reflects the distribution of galaxies in the cluster.

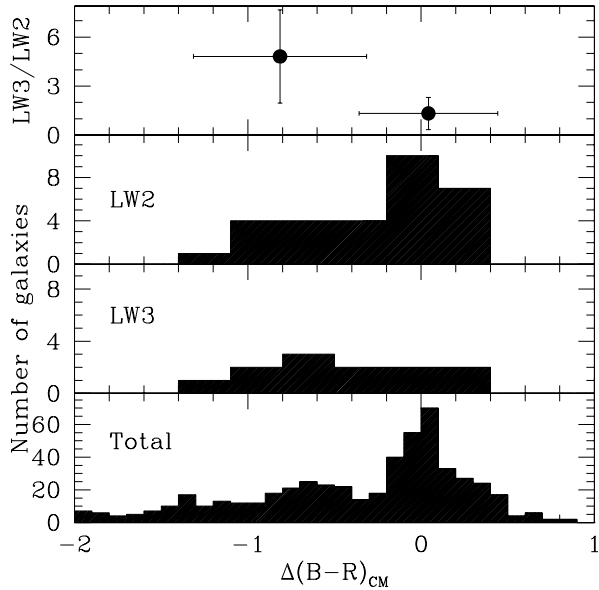


Fig. 10. On the bottom: distributions of differences between the B-R color of galaxies and the B-R color expected from the B magnitude if the galaxy would obey the color-magnitude relation. The LW2 distribution does not differ from the global galaxy distribution, while LW3 distribution does not show a peak corresponding to the color-magnitude relation. On the top: the mean color of sources emitting in the two filters versus the distance from color-mag relation in the B-R plane. Outliers of the color-mag relation have a LW3/LW2 mean color bigger than sources in the color-mag relation.

On the contrary, the emission in the LW3 band seems to increase with distance from the cluster center. In the case of our confirmed members, we have a significant correlation between LW3 flux and distance to the center (the classical Spearman correlation coefficient, $\rho_S = 0.52$, has the high 92% significance). We have also explored the color LW3/LW2 of sources detected in the LW2 and LW3 band, using upper limits when sources are not detected in one of the bands. We see that the mean color LW3/LW2 of LW3 detected galaxies increases with the distance to the cluster center while that of LW2 galaxies is almost constant. This behavior is consistent with the spatial distribution of starburst galaxies and blue galaxies responsible for the Butcher-Oemler effect. Therefore, we can conclude that selecting galaxies which emit in the LW3 band allows one to emphasise star formation galaxies.

4.2. Color distribution

Do the galaxies which emit in the MIR have peculiar optical signatures? To answer this question we have studied the optical colors of these galaxies with respect to the colors of the other cluster galaxies (see Fig. 10). Colors and magnitudes of early-type galaxies in galaxy clusters are strongly correlated (Visvanathan & Sandage, 1977). Galaxies which do not obey this correlation are believed to be late type or peculiar. In particular, the blue outliers of this relationship are responsible for the Butcher-Oemler effect. To enhance the position of ISOCAM

galaxies in the color-magnitude plot, we have fitted the color-magnitude relation of A1689 by using a $k\text{-}\sigma$ clipping technique (see Duc et al., 2000) and then we have computed, for each galaxy, the difference between its B-R color and the color given by the color-magnitude relation at the B magnitude of the galaxy. Fig. 10 shows the distribution of these relative colors for the detected LW2 and LW3 galaxies and for all the optical galaxies in the region observed by ISOCAM (total). The figure showing the total distribution has a peak at zero which corresponds to the galaxies obeying the color-magnitude relation.

While the distribution of LW2 galaxies is similar to the total one, the LW3 distribution clearly misses the peak due to the color-magnitude relation and most of the LW3 detections are blue-outliers of the relation which are supposed to be responsible for the Butcher-Oemler effect.

Finally, if we consider the galaxies detected in the two filters (see the top of Fig. 10), the mean LW3/LW2 color of the galaxies obeying the color-magnitude relation is smaller than that of the blue-outliers.

We can easily explain the absence of LW3 detections in the peak because early-type galaxies are rarely detected with the LW3 filter (see Fig. 8) except for very bright galaxies in the center of the cluster where the observations are highly sensitive. On the other hand, the blue color and the high LW3/LW2 flux ratio of most of the LW3 detected galaxies imply that some of the blue galaxies responsible for the Butcher-Oemler effect harbor hidden star formation, as revealed by dust emission. The color of these galaxies is still bluer than the color-magnitude relation because only part of the young stars is hidden by dust (see e.g. Poggianti et al., 1999).

4.3. Comparison with local clusters and field galaxies

Galaxies detected in the LW2 band correspond to the brightest optical sources, which results in an overdensity in the cluster region with respect to the field.

On the other hand, the density of galaxies detected in the LW3 band in the A1689 region is clearly in excess with respect to the field. By considering the 100% completeness limit of 0.6 mJy, the expected number of sources brighter than this limit in an area of 20 square arcminutes is 3_{-1}^{+2} , according to the integral counts of Elbaz et al. (1999), while we find 9 galaxies above this flux, 5 of them are cluster members. If we consider fluxes greater than 0.4 mJy (the 90% completeness limit), we expect 7_{-2}^{+3} background galaxies while we find 14 galaxies, 9 of them are cluster members.

We compare in this paragraph the MIR fluxes and MIR/optical flux ratios of the A1689 galaxies with the galaxies detected in local clusters and in the field. Our goal is to detect an eventual excess of bright LW3 sources in A1689 with respect to local rich clusters. In fact, according to previous IRAS studies of nearby clusters (see e.g. Bica & Giovanelli, 1987; Wang et al., 1991), almost only “IR-normal” galaxies have been detected in clusters in contrast to the field where at least 20% have FIR luminosities $> 10^{11} L_{\odot}$. Unfortunately, only a few such clusters have been observed in the MIR with ISOCAM.

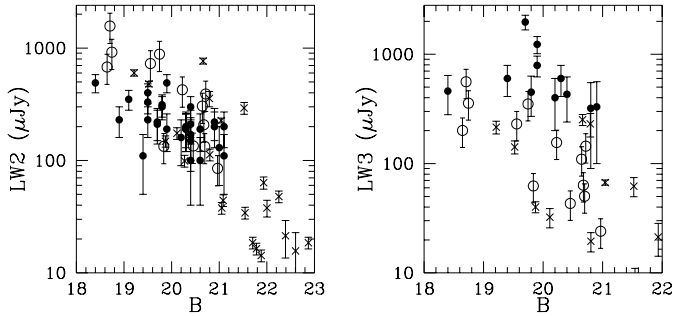


Fig. 11. Comparison of fluxes of A1689 galaxies (filled circles) with those of Coma galaxies (empty circles) and Virgo galaxies (crosses) placed at the distance of A1689, as a function of their B magnitude. We note that, in the LW3 band, A1689 galaxies are on average brighter than local cluster galaxies.

Boselli et al. (1997) have studied a complete sample of late-type and S0 galaxies brighter than $B_T \leq 18$ in the Virgo cluster. For our comparison we use the subsample of 27 galaxies observed in a circle of 2 degrees centered on M87, which corresponds to ~ 0.5 Mpc, almost the same as in our ISOCAM observations. For most of the galaxies in this region we used a new estimate of the fluxes as obtained by Roussel et al. (2000).

A sample of 13 spiral and irregular galaxies within 1 degree (~ 1.5 Mpc) of the Coma cluster center has been studied by Contursi (1999). The galaxies of the sample have been selected among the galaxies detected by IRAS at $60\mu\text{m}$ with blue colors ($B - H \leq 2.75$). The sample, although not complete, can be taken as representative of the more active galaxies in the cluster. Moreover, a sample of seven E+A galaxies has been observed in Coma by Quillen et al. (1999). These galaxies appear to be fainter than the late-type galaxies observed by Contursi (1999), which is in agreement with their small contribution to the total FIR emission estimated by Quillen et al. (1999).

Fig. 11 shows the comparison of the MIR fluxes of A1689 galaxies with those of Virgo and Coma galaxies, placed at the distance of A1689 by computing the K-correction on the basis of the MIR SED of the photo-dissociation region NGC 7023 (Cesarsky et al., 1996b; see Fig. 8). While the distribution of LW2 fluxes is similar for the three clusters, in the LW3 band A1689 galaxies appear brighter than galaxies in the local clusters. The use of the SED of a starburst galaxy would increase this effect.

A direct comparison of luminosity functions of the three cluster samples, to deduce if there is a real excess of luminous $15\mu\text{m}$ sources in A1689 with respect to local clusters, is difficult. In particular, it is difficult to correct luminosity functions for incompleteness, due to the optical selection of galaxies in the local clusters. Moreover, this comparison is affected also by the small size of the samples and the different cluster richness.

To overcome these problems, we have explored the ratio of MIR to optical fluxes of the galaxies in the central region of the clusters (radius of 0.5 Mpc), which is relatively free of sample selection. Moreover, since in this region, which corresponds to the A1689 field observed by ISOCAM, the bright end of Coma

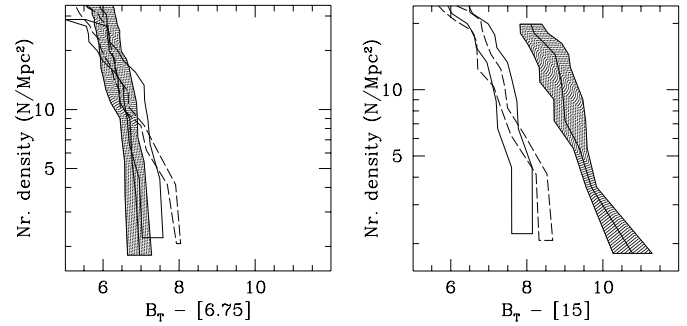


Fig. 12. Comparison among the cumulative distributions of the MIR/optical fluxes for galaxies in the central region ($R < 0.5$ Mpc) of Virgo (dashed line), Coma (continuous line) and A1689 (hatched region) clusters. Coma and Virgo distributions are scaled at the richness of A1689 using their velocity dispersions as richness parameter. The $B_T - [6.75]$ color distributions (left) of the three clusters do not differ significantly. The $B_T - [15]$ color distribution (right) of A1689 shows an excess of galaxies with high $B_T - [15]$ colors with respect to the other two local clusters, which have a similar behavior.

and Virgo MIR luminosity functions are well sampled, we can scale the cumulative distributions with respect to the richness of the clusters. In this way it is possible to also detect an excess in the density of luminous sources. To do so, we scale the distributions at the richness of A1689 using the velocity dispersions of the clusters, by exploiting the linear relationship between the velocity dispersion and the richness of galaxy clusters within 0.5 Mpc (Bahcall 1981). We use the values of $\sigma_r = 632_{-29}^{+41}$, 821_{-38}^{+49} , 1429_{-96}^{+145} for Virgo, Coma and A1689 velocity dispersions, respectively (Fadda et al. 1996, Girardi et al. 1997).

We have transformed MIR fluxes in magnitudes using the relationships of Omont et al. (1999):

$$\text{mag}(LW2) = [6.75] = 12.39 - 2.5 \log[F_{LW2}(mJy)]$$

$$\text{mag}(LW3) = [15] = 10.74 - 2.5 \log[F_{LW3}(mJy)]$$

In order to put the galaxies of Coma and Virgo at the distance of A1689, we have applied a K-correction to the B fluxes of Virgo and Coma galaxies according to Poggianti (1997).

Fig. 12 shows that the distributions of $B_T - [6.75]$ colors are similar for the three clusters, while the $B_T - [15]$ color distribution of A1689 differs significantly from that of the other two clusters. A1689 shows an excess of galaxies with steep spectra with respect to Coma and Virgo clusters. If we remember that LW3 sources correspond to blue outliers of the color-magnitude relation of A1689 galaxies, we can conclude that the LW3 emission is a very sensitive indicator of star formation. A kind of analog of the optical Butcher-Oemler effect is clearly revealed by the ISO observations.

Finally, we have compared the galaxies of A1689 detected in the LW3 band with field galaxies located at a similar redshift (Fig. 13). In this perspective, we used a sample of galaxies observed in the Canada France Redshift Survey field CFRS-0300 (Flores et al. 2000) located at redshifts between 0.1 and 0.3 in order to obtain sufficient statistics.

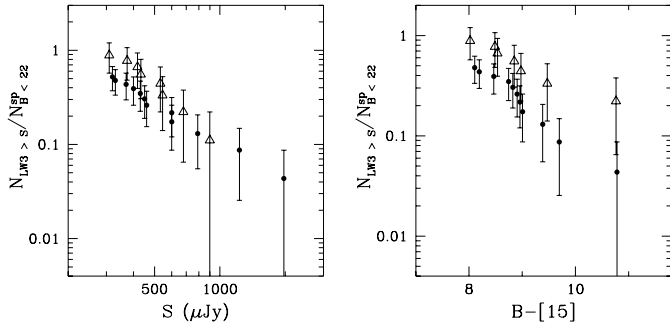


Fig. 13. Comparison between LW3 fluxes (left) and LW3/optical colors (right) of A1689 (full circles) and CFRS galaxies (empty triangles) within the redshift range 0.1–0.3. The cumulative distributions are normalized to the number of spirals with $B < 22$ in the observed areas. Poissonian error bars are shown.

Since most of the sources which emit in the LW3 band at this redshift are spiral or irregular galaxies, we have normalized the distributions to the number of spiral/irregular galaxies in the field and in the cluster with $B < 22$. In this way, we take out the effect of the morphology-density relation. For the field galaxies, we used the percentage of spiral/irregular galaxies in the CFRS fields according to Brinchmann et al. (1998). For A1689, we used HST morphologies (Couch, private communication) and the spectroscopic redshifts by Dye et al. (2000) in the field observed by ISOCAM.

The two distributions are compatible within the error bars. This means that the $15 \mu\text{m}$ luminosities and the $B-[15]$ colors of A1689 galaxies detected in the LW3 band are similar to those of field galaxies at the same redshift.

$15 \mu\text{m}$ sources are typically spiral galaxies which constitute 20% of the total population of A1689 galaxies and 50% of field galaxies at the redshift of the cluster. On the other hand, by comparing counts in the V band of field galaxies and galaxies in the central region of A1689, Wilson et al. (1997) find an overdensity of a factor two for $V < 22$. Since we find a clear overdensity of $15 \mu\text{m}$ sources in the cluster with respect to the field, we can say that the environment of A1689 likely triggers starburst episodes in galaxies in the cluster outskirts, although the overall properties (infrared luminosities and FIR/optical colors) of these are similar to field starburst galaxies.

4.4. Diffuse IR emission

In this section we address the issue of the possible presence of diffuse infrared emission due to intra-cluster dust. Theoretically it is difficult to understand how such intra-cluster infrared emission could originate from the central region of rich and well evolved galaxy clusters since the timescale for the destruction of dust grains shocked by the hot X-ray plasma of electrons (sputtering) is of the order of a few 10^8 years (Dwek et al. 1990). Only dust replenishment by galactic winds or by stripping of in-falling galaxies could explain such emission but it is not expected to happen in the central Mpc of rich clusters. However, a systematic study of 56 clusters of galaxies using IRAS data led

Table 4. Measured background values compared with zodiacal light previsions using DIRBE measurements. Almost all the background emission can be explained with zodiacal light.

Solar Elongation (deg)	Filter	Zod. light (model) (MJy/sr)	Background (MJy/sr)
71.5	LW2	9.5	9.7 ± 0.2
71.5	LW3	64.6	54.5 ± 0.6
104.6	LW3	39.5	34.5 ± 0.4
108.6	LW2	4.3	4.7 ± 0.1
72.9	C200	3.8	4.0 ± 0.2

Table 5. Estimates of the emission in several PHOT bands in the FIR by galaxies brighter than 0.2 mJy in the LW2 band and than 0.5 mJy in the LW3 band.

PHOT band	FIR (LW2 > 0.2mJy) (MJy/sr)	FIR (LW3 > 0.5mJy) (MJy/sr)
$120 \mu\text{m}$	0.22	0.24
$175 \mu\text{m}$	0.14	0.16
$200 \mu\text{m}$	0.09	0.11

Wise et al. (1993) to suggest detections for intracluster emission in two clusters. More recently Stickel et al. (1998) claimed to have detected intracluster dust emission in the central region of Coma using ISOPHOT at $120 \mu\text{m}$.

Since A1689 and Coma have similar properties, one may expect similar diffuse emission in the two clusters. We have measured the diffuse emission in the field of A1689 in three bands: LW2 and LW3 with ISOCAM and at $200 \mu\text{m}$ with ISOPHOT. In Table 4, we compare our values with the expectations based on a model of the zodiacal background light using the DIRBE observations (B. Reach, private communication). All three values agree well with the DIRBE estimates for this region.

Unfortunately A1689 is very close to the ecliptic plane (at an ecliptic latitude of $\beta = 5.78$ degrees) where the infrared background due to diffracted solar light is very high. Hence if a small intra-cluster contribution were present it would be very difficult to detect. In particular, a FIR background light of 0.1 MJy/sr as proposed by Stickel et al. (1998) for Coma is still compatible with our error bars. However, we can use the MIR flux densities of the A1689 galaxies resolved with ISOCAM to deduce their contribution to the FIR background light assuming a given FIR over MIR ratio. We report this contribution in Table 5 using the ratio reported by Contursi (1999) for the Coma galaxies for which there is both ISOCAM MIR and IRAS FIR measurements. We find values of the order of the measurement of Stickel et al. (1998), in agreement with Quillen et al. (1999) for Coma. Hence, our results agree with the conclusion of Quillen et al. (1999): the origin of the FIR background light in the direction of rich clusters is most probably due to the integrated contribution of the cluster galaxies.

5. Summary and conclusions

We have presented the results of infrared observations of Abell 1689, an exceptionally rich cluster of galaxies at intermedi-

ate redshift ($z \simeq 0.181$), with ISOCAM, at 6.7 and 15 μm , and ISOPHOT at 200 μm , from the *Infrared Space Observatory* (ISO).

The ISOCAM observations, which cover a region of 20 square arcminutes, reach a sensitivity limit of 0.15 mJy at 6.7 μm and 0.3 mJy at 15 μm . From a spectroscopic follow-up (Duc et al. 2000) and a set of photometric redshifts (Dye et al. 2000) we know redshifts for all the galaxies except one. This has allowed us to explore the infrared properties of cluster members within a radius of ~ 0.5 Mpc.

Galaxies detected in the LW2 band, which is mostly dominated by stellar emission, correspond to the brightest optical objects. They appear concentrated in the central part of the cluster and show optical colors similar to those of the overall cluster population.

The cluster members detected in the LW3 band are blue outliers of the cluster color-magnitude relation and become brighter going from the center to the outer parts of the cluster.

We have estimated the cumulative distributions of the ratios of MIR to optical fluxes in the two bands above the 90% completeness limits of 0.2 mJy for LW2 and 0.4 mJy for LW3. Comparing these distributions to those of the two nearby galaxy clusters, Virgo and Coma, scaled at the richness of A1689, we find that they are compatible in the LW2 filter. On the contrary, Abell 1689 shows a systematic excess of galaxies detected at 15 μm with high 15 μm to optical ratio indicating higher star formation activity. Therefore, the far-infrared shows a trend similar to the Butcher-Oemler effect measured in the optical. The case of A1689 is even more remarkable since it shows an excess of activity in the cluster galaxy population at $z \sim 0.2$ with respect to nearby clusters which is still debated on the basis of optical data (Gudehus & Hegyi 1991). A comparison with field galaxies observed in the LW3 band at the redshift of A1689 shows that, in the limits of our fairly large error bars, cluster galaxies are not more luminous and more active than field galaxies.

Moreover, we find a clear overdensity of 15 μm sources in the cluster with respect to the field while optical counts of spiral galaxies which mainly emit at 15 μm do not show this overdensity. Therefore, we can say that the environment of A1689 likely triggers starburst episodes in galaxies in the cluster outskirts, although the overall properties (infrared luminosities and far-infrared/optical colors) of these are similar to field starburst galaxies.

The spatial resolution of ISOPHOT is too poor to study the galaxy population. We used it to calculate the integrated FIR background light of the cluster and compared it to the expected contribution of the individual galaxies, evaluated using their MIR luminosities and assuming a FIR/MIR ratio based on Coma galaxies. We find no evidence for intra-cluster dust emission in the limit of our error bars, whereas the integrated FIR light produced by the individual galaxies seems sufficient to produce an integrated FIR flux at a level similar to that previously reported for the Coma cluster.

Acknowledgements. We thank René Gastaud and Hervé Aussel for help with the data reduction of the ISOCAM images, Guilain Lagache and Marc Sauvage for their advice on ISOPHOT data reduction and

Bianca Maria Poggianti and Suzanne Madden for interesting discussions and suggestions when we were writing the manuscript. We are also grateful to Bill Reach for relevant values of zodiacal light produced by his model, to Warrick J. Couch who provided us the HST morphologies of A1689 galaxies prior to publication and to Simon Dye who gave us their photometric redshifts. We thank the referee Ian Smail for his careful reading of the manuscript and his helpful suggestions. P.-A. D. acknowledges support from the network Formation and Evolution of Galaxies set up by the European Commission under contract ERB FMRX-CT96086 of its TMR program.

References

- Abraham R.G., Smecker-Hane T.A., Hutchings J.B., et al., 1996, *ApJ* 471, 694
- Altieri B., Metcalfe L., Kneib J.P., 1999, *A&A* 343, L65
- Aussel H., Cesarsky C.J., Elbaz D., Starck J.L., 1999, *A&A* 342, 313
- Bahcall N.A., 1981, *ApJ* 247, 787
- Balogh M.L., Schade D., Morris S.L., et al., Carlberg R.G., Ellingson E., 1998, *ApJ* 504, 75
- Balogh M.L., Morris S.L., Yee H.K.C., Carlberg R.G., Ellingson E., 1999, *ApJ* 527, 54
- Bicay M.D., Giovanelli R., 1987, *ApJ* 321, 645
- Biviano A., Girardi M., Giuricin G., Mardirossian F., Mezzetti M., 1992, *ApJ* 396, 35
- Biviano A., Katgert P., Mazure A., et al., 1997, *A&A* 321, 84
- Biviano A., Sauvage M., Gallais P., et al., 1999, *Experimental Astronomy*. in press (astro-ph/9910297)
- Boselli A., Lequeux J., Contursi A., et al., 1997, *A&A* 324, L13
- Brinchmann J., Abraham R., Shade D., et al., 1998, *ApJ* 499, 112
- Butcher H., Oemler A., 1978, *ApJ* 219, 18
- Butcher H., Oemler A., 1984, *ApJ* 285, 426
- Carlberg R.G., Yee H.K.C., Ellingson E., et al., 1997, *ApJ* 476, L7
- Cesarsky C.J., Abergel A., Agnese P., et al., 1996a, *A&A* 315, L32
- Cesarsky D., Lequeux J., Abergel A., et al., 1996b, *A&A* 315, 305
- Charmandaris V., Laurent O., Mirabel I.F., et al., 1999, *Ap&SS* 266, 175
- Contursi A., 1999, Ph.D. Thesis, ed. by CEA, Saclay
- Couch W.J., Newell E.B., 1984, *ApJS* 56, 143
- Couch W.J., Sharples R.M., 1987, *MNRAS*, 229, 423
- Coulais A., Abergel A., 1999, In: Cox P., Kessler M.F. (eds.) *The Universe as seen by ISO*. ESA SP-427, p. 61
- Downes A.J.B., Peacock J.A., Savage A., Carrie D.R., 1986, *MNRAS* 218, 31
- Dressler A., 1980, *ApJS* 42, 565
- Dressler A., Gunn J.E., 1992, *ApJS* 78, 1
- Dressler A., Gunn J.E., Schneider D.P., 1985, *ApJ* 294, 70
- Dressler A., Smail I., Poggianti B.M., et al., 1999, *ApJS* 122, 51
- Duc P.A., Fadda D., Flores H., et al., 2000, in preparation
- Dwek E., Rephaeli Y., Mather J., 1990, *ApJ* 475, 565
- Dye S., Taylor A.N., Thommes E.M., et al., 2000, *MNRAS* submitted, astro-ph/0002011
- Elbaz D., Cesarsky C., Fadda D., et al., 1999, *A&A* 351L, 37
- Ellingson E., Lin H., Yee H.K.C., Carlberg R.G., 1999, to appear in: Bunker A.J., van Breugel W.J.M. (eds.) *The Hy-Redshift Universe*. PASP Conf. Ser. in press, astro-ph/9909074
- Fadda D., Elbaz D., 1998, In: Cox P., Kessler M.F. (eds.) *The Universe as seen by ISO*. ESA SP-427, p. 1037
- Fadda D., Girardi M., Giuricin G., et al., 1996, *ApJ* 473, 670
- Flores H., Hammer F., Thuan T.X., et al., 1999, *ApJ* 517, 148
- Flores H., Hammer F., Thuan T.X., et al., 2000, in preparation

- Fujita Y., Nagashima M., 1999, *ApJ* 516, 619
Gavazzi G., Jaffe W., 1987, *A&A* 186, 1
Ghigna S., Moore B., Governato F., et al., 1998, *MNRAS* 300, 146
Girardi M., Fadda D., Escalera E., et al., 1997, *ApJ* 490, 56
Gudehus D.H., Hegyi D., 1991, *AJ* 101, 18
Gunn J.E., Gott J.R. III, 1972, *ApJ* 176, 1
Hewett P.C., Foltz C.B., Chaffee F.H., 1995, *AJ* 109, 1498
Kessler M.F., Steinz J.A., Anderegg M.E., et al., 1996, *A&A* 315, 27
Lavery R.J., Henry J.P., 1986, *ApJ* 304, 5
Lemke D., Klaas U., Abolins J., et al., 1996, *A&A* 315, L64
Lubin L.M., 1996, *AJ* 112, 23
Madden S.C., Vigroux L., 1999, In: Carral P., Cepa J. (eds.) *Star Formation in Early Type Galaxies*. ASP Conf. Ser. 163, p. 135
Margoniner V.E., de Carvalho R.R., 2000, *AJ* 119, 1562
Moore B., Katz N., Lake G., Dressler A., Oemler A. Jr., 1996, *Nat* 379, 613
Omont A., Ganesh S., Alard C., et al., 1999, *A&A* 348, 755
Poggianti B.M., 1997, *A&AS* 122, 399
Poggianti B.M., Smail I., Dressler A., et al., 1999, *ApJ* 518, 576
Poggianti B.M. & Wu H., 2000, *ApJ* 529, 157
Quillen A.C., Rieke G.H., Rieke M.J., Caldwell N., Engelbracht C.W., 1999, *ApJ* 518, 632
Rakos K., Odell A., Schombert J., 1997, *ApJ* 490, 194
Rakos K.D., Schombert J.M., 1995, *ApJ* 439, 47
Ramirez A.C., de Souza R.E., 1998, *ApJ* 496, 693
Rigopoulou D., Franceschini A., Genzel R., et al., 1999, to appear in: Lemke D., Stickel M., Wilke K. (eds.) *ISO Surveys of a Dusty Universe*. astro-ph/9912544
Roussel H., Vigroux L., Sauvage M., et al., 2000, in preparation
Sanders D.B., Mirabel I.F., 1996, *ARA&A* 34, 749
Smail I., Morrison G., Gray M.E., et al., 1999, *ApJ* 525, 609
Starck J.-L., Aussel H., Elbaz D., Fadda D., Cesarsky C., 1999, *A&AS* 138, 365
Stickel M., Lemke D., Mattila K., Haikala L.K., Hass M., 1998, *A&A* 329, 55
Struble M.F., Rood H.J., 1987, *ApJS* 63, 543
Teague P.F., Carter D., Gray P.M., 1990, *ApJS* 72, 715
Tran D., 1998, Ph.D. Thesis, ed. by CEA, Saclay
Visvanathan N., Sandage A., 1977, *ApJ* 216, 214
Wang G., Leggett S.K., Clowes R.G., MacGillivray H.T., Savage A., 1991, *MNRAS* 248, 112
Wilson G., Smail I., Ellis R.S., Couch W.J., 1997, *MNRAS* 284, 915
Wise M.W., O'Connell R.W., Bregman J.N., Roberts M.S., 1993, *ApJ* 405, 94